# THE EFFECT OF FLOW RATE, HEAD POSITION, AND INHALER ORIENTATION ON THE AIRFLOW AND PARTICLE DEPOSITION IN AN MRI-BASED MOUTH-THROAT GEOMETRY

**Fotos S. Stylianou, Stelios I. Angeli, and Stavros C. Kassinos**

Computational Sciences Laboratory (UCY-CompSci)
Department of Mechanical and Manufacturing Engineering
University of Cyprus
University Avenue 1, Nicosia 2109, Cyprus
stylianou.fotos@ucy.ac.cy, angeli.stelios@ucy.ac.cy, kassinos@ucy.ac.cy

**Mårten Svensson**

Emmace Consulting AB
Medicon Village
SE-223 81 Lund, Sweden
marten@emmace.se

## ABSTRACT

The mouth-throat plays a key role in the administration of inhaled medicines. It is an area of intense filtration, where an unacceptably high fraction of the released drug dose is deposited and thus wasted. Due to the relatively high flow rate associated with Dry Powder Inhalers (DPIs), drug particles are released at a high velocity, which causes substantial deposition in the oral cavity and the throat region by inertial impaction. Hence, reducing the mouth-throat deposition is of utmost importance and this can only be achieved by designing more efficient inhaler devices (functioning at lower flow rates) and by obtaining a better understanding of the mechanisms that cause the oropharyngeal losses.

The present study is designed to identify the main factors that determine aerosol deposition (unwanted filtering) in the mouth-throat region, with the aim of controlling the leading effects that contribute to the oropharyngeal deposition losses for drugs delivered via DPIs. For this reason micron-sized particles are released and tracked in a patient-specific MRI-based mouth-throat geometry under three inhalation flow rates (15L/min, 30L/min, 60L/min), three head positions (straight, up, left), and three inhaler mouthpiece orientations ($0^o$, $15^o$, $30^o$). Direct Numerical Simulations (DNS) are performed for the low flow rate using prescribed laminar inlet conditions, while Large Eddy Simulations (LES) are performed for the intermediate and high flow rates using fully-developed turbulent inlet conditions.

Interestingly, our results reveal that the deposition fraction is insensitive to the head position, whilst the inhalation flow rate and the inhaler mouthpiece orientation have a strong influence on the aerosol deposition in the mouth-throat region. Furthermore, we illustrate the mean flow structures and examine their effect on the particle deposition of various micron sizes. Despite the fact that our results are case specific, we expect the main trends to be universal.

## INTRODUCTION

Pulmonary delivery is emerging as a promising drug administration method for medicines. In the case of respiratory ailments, inhalation provides the shortest and most direct route to the target site, thus minimizing side effects and maximizing effectiveness. In the case of systemic diseases, pulmonary delivery often offers a fast administration mode (second only to injection) and other significant benefits, such as a large surface area for deposition and absorption, and limited enzymatic activity as compared to the gastrointestinal route (Patton *et al.*, 2004). Despite these significant advantages and the promise held, a number of problems hinder wider adoption of inhalation as a primary administration route. One of these problems, which forms the subject of the present study, is the unacceptably high fraction of the released drug dose that never reaches its target site.

The mouth-throat plays a key role during pulmonary drug delivery. It is an area of intense filtration, where a sizable portion of the released drug is deposited and thus never reaches the conducting and respiratory airways. In fact, drug deposition in the targeted area of the lung (typically the lower respiratory tract) from currently marketed DPIs is roughly between 7.5% and 40% of the label claim, depending on the inhaler design and type of formulation used (Usmani *et al.*, 2005; Demoly *et al.*, 2014; de Boer *et al.*, 1996; DeHaan & Finlay, 2004). It is only for some carrier-free drug formulations that higher lung deposition fractions (up to 40% of the label claim) have been reported (Behara *et al.*, 2014). It is evident that, drug losses in the mouth-throat region remain at unacceptably high levels (often more than 50%), especially for DPIs.

## METHODOLOGY AND IMPLEMENTATION

To generate physiologically realistic mouth-throat geometries under three head positions (head-straight, head-up, head-left), the first author (Sex: male, Age: 32y, Height: 1.76m, Weight: 74Kg) was subjected to MRI scanning at the Prognosis Advanced Diagnostic Center, where the second author is occupied as a Medical Physicist. During the three MRI scans, a DPI mouthpiece was held between the lips of the subject, emulating the proper opening of the mouth-throat during inhalation from an inhaler. Great care was taken during the MRI scan of the head-straight position, in order to produce clear images of sufficient quality. The same was not achieved for the head-up and head-left positions, due to the inconvenient head posture inside the head-neck MRI coil, which prompted frequent swallowing, leading to blurry images.

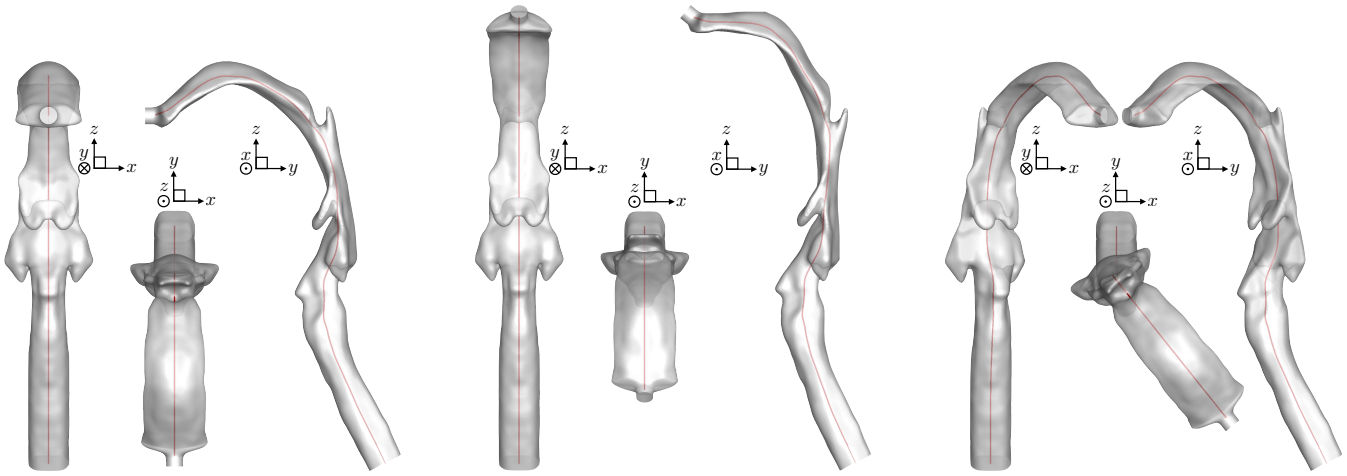


Figure 1: Front, top, and side view points for each of the three distinct head positions: (a) head-straight, (b) head-up, (c) head-left.

The three MRI data sets were processed with the Simpleware ScanIP software and 3D mouth-throat models were generated. Great effort was put during the 3D reconstruction of the mouth-throat model with head-straight position (Figure 1a), while for the head-up and head-left positions only crude models were constructed as a result of the aforementioned blurriness in the MRI images. Note that left-right symmetry was applied to the MRI data of the head-straight position in order to increase the quality of the data and to produce a symmetric model. The final mouth-throat models with head-up (Figure 1b) and head-left (Figure 1c) positions were obtained from geometric transformations of the head-straight model. In this process the aforementioned crude models were used as guidance. Prior to the geometric transformations, a skeletonization process was applied on the head-straight model, which resulted into a representative line for the 3D model (see Figure 1). Rotational transformations, spread across specific regions of the skeleton line, were used to convert the head-straight model into head-up ($x$-axis rotations, with cumulative rotation angle $-39.10^{\text{o}}$) and head-left ($z$-axis rotations, with cumulative rotation angle $+38.55^{\text{o}}$) models.

To assess the effect of the inhaler orientation on the mouth-throat airflow and particle deposition, three distinct inlet parts were designed and merged with the head-straight mouth-throat model. Figure 2 illustrates the three inlet orientations adopted (i.e. $0^{\text{o}}$, $15^{\text{o}}$, $30^{\text{o}}$). For the head-up and head-left mouth-throat models the three inlet parts are subjected to the rotational transformations described in the previous paragraph. Thus the relative orientation of an inlet part with the lips is the same in all three head positions.

In addition to the three head positions and the three inhaler orientations, three inhalation flow rates are also adopted (i.e. $Q$=15/30/60L/min). Based on the airflow properties (kinematic viscosity $\nu_f$=1.6601×10$^{-5}$m$^2$/s and density $\rho_f$=1.1422Kg/m$^3$ at body temperature $T$=36$^{\text{o}}$C), the inlet dimensions (circular cross sectional area $A=\pi R^2$ with radius $R$=4mm), and the three inhalation flow rates $Q$, the corresponding bulk Reynolds numbers $Re_b=\frac{2Q}{\nu\sqrt{\pi A}}$ are $Re_b\approx$2397/4794/9587. The associated bulk velocities $u_b=\frac{\nu Re_b}{2R}$ are $u_b\approx$4.97/9.95/19.89m/s. For the low inhalation rate, the associated bulk Reynolds number falls into the laminar regime and thus we use fully developed laminar inlet conditions. On the contrary, for the intermediate and high flow rates the associated bulk Reynolds numbers fall into the turbulent regime. For these cases, we use fully developed turbulent inlet profiles based on a recycling boundary condition scheme. The implementation of this scheme demands the extrusion of the inlet section for a total length of $L_e$=30$R$, with the recycling length set to $L_r$=15$R$. In all cases the convective outlet boundary condition is employed. Although the selected inlet profiles may not be fully representative of those generated from commercial inhalers, they still should be sufficient to highlight the relative differences between the mouth-throat deposition induced from the various combinations of flow rate, head position, and inhaler orientation.

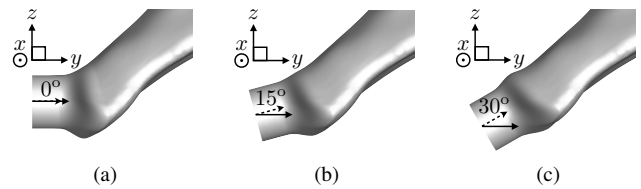


Figure 2: Three inlet orientations emulating three different angle positions of an inhaler mouthpiece between the lips.

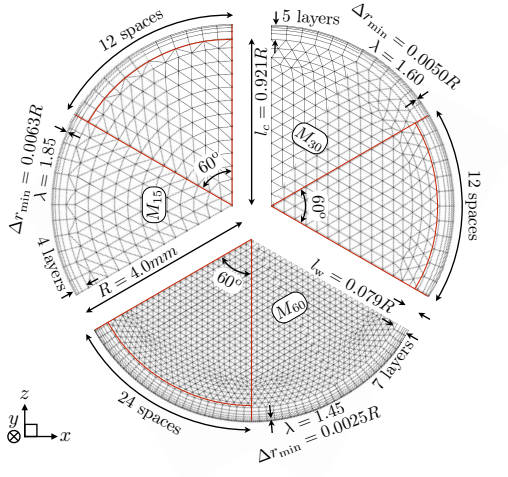


Figure 3: Grid details at the inlet for the 3 mesh densities considered (i.e. $M_{15}$, $M_{30}$, $M_{60}$). Note that $\Delta r_{\text{min}}$ is the first grid node from the wall, and $\lambda$ is the average expansion ratio of the wall layers.

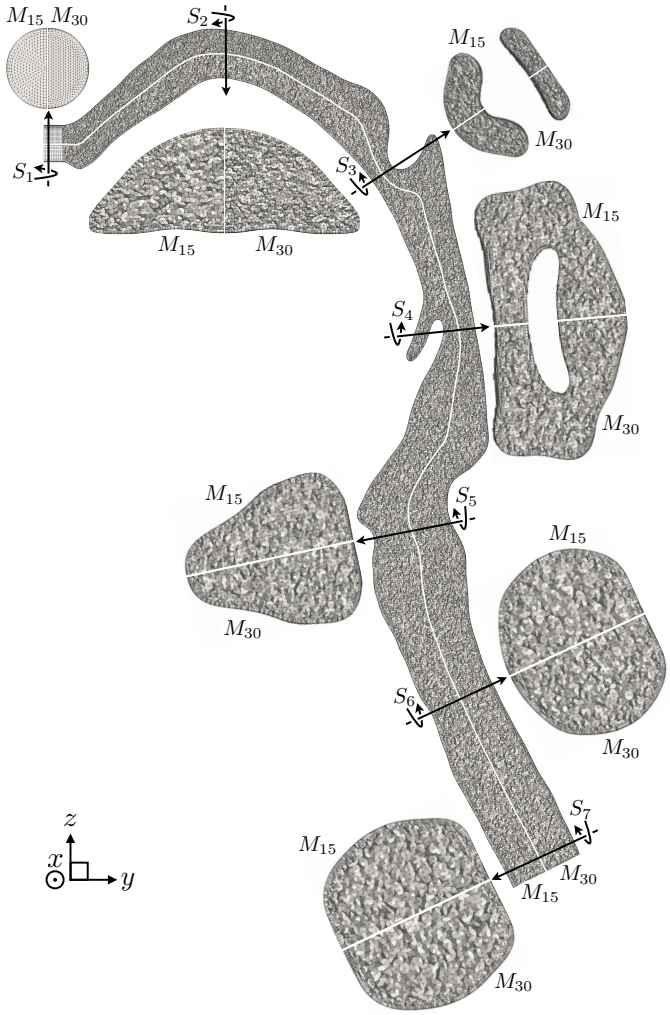


Figure 4: Mesh resolution comparison between $M_{15}$ and $M_{30}$ at eight cross sections (i.e. one at the symmetry plane and seven normal to this plane). The $S_1$-$S_7$ cross sections are slightly scaled with respect to the symmetry plane section.

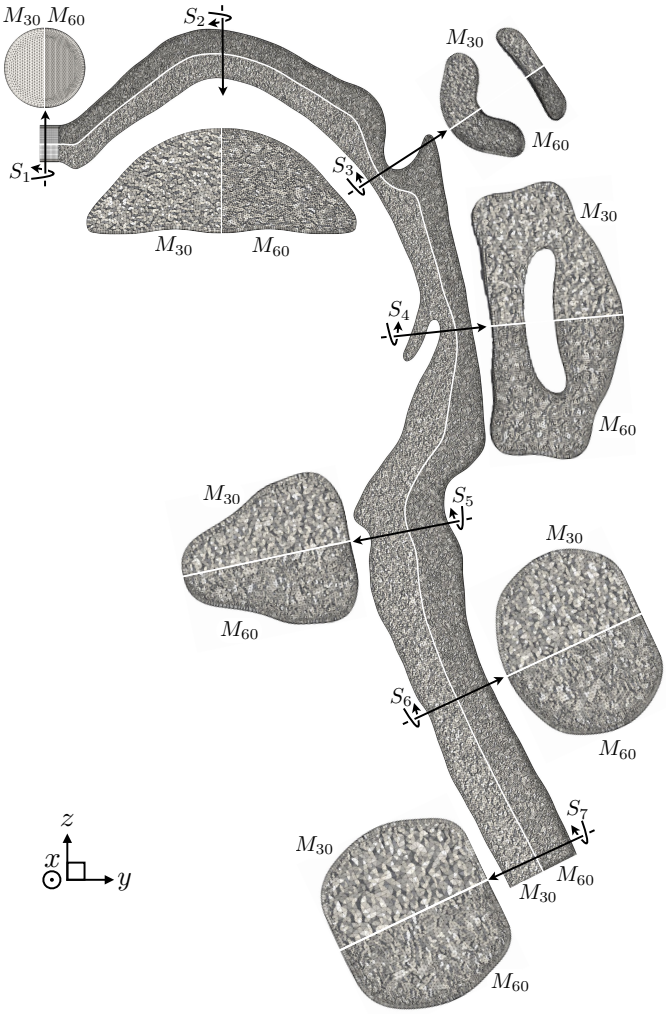


Figure 5: Same as in Figure 4, but here the mesh resolution comparison is between $M_{30}$ and $M_{60}$.

To simulate the low, intermediate, and high flow rates we have generated grids with three mesh densities, namely: $M_{15}$, $M_{30}$, and $M_{60}$. Figure 3 delineates the grid details of these meshes at the inlet, while Figures 4 and 5 display a comparative mesh resolution at various cross sectional areas of the domain for $M_{15}$-$M_{30}$ and $M_{30}$-$M_{60}$, respectively. The near wall region is resolved with prismatic elements, while the core of the domain is meshed with tetrahedral elements. The number of grid cells involved in $M_{15}/M_{30}/M_{60}$ is $8.7/10.5/44.4$ millions. The $M_{30}$ is obtained via local refinement of $M_{15}$, with a relative increase of grid cells in the volume between stations: $S_1$-$S_3$ of 33.5%, $S_3$-$S_5$ of 16.3%, and $S_5$-$S_7$ of 9.8%. Note that the number of prism layers increases from 4 to 5. The $M_{60}$ is obtained via pure refinement of $M_{30}$, with the exception of the near wall region where the number of prism layers increases from 5 to 7. Noteworthy of mention is that $M_{30}$ has been constructed *a posteriori* of the low and intermediate flow rate simulations that used $M_{15}$, while the $M_{60}$ has been constructed *a posteriori* of the high flow rate simulation that used $M_{30}$. To assess the grid-independence of our results, we are currently simulating the intermediate and high flow rates using the $M_{30}$ and $M_{60}$, respectively.

The turbulent inlet conditions, for the intermediate and high flow rates, are accommodated via the extrusion length $L_e$=30$R$ in which the inlet mesh of $M_{15}/M_{30}/M_{60}$ is repeated for $10/15/20$ layers for every streamwise distance of length $1R$. Based on the friction velocity $u_\tau$ at the inlet pipe section, the friction Reynolds numbers $Re_\tau=\frac{u_\tau R}{\nu}$ for the three flow rates are approximately $Re_\tau\approx 70/165/300$. For the intermediate flow rate, the viscous length unit $\delta=\nu_f/u_\tau$ at the inlet is $\delta\approx 0.00606R$ and thus the near wall radial, circumferential, and streamwise spacings for $M_{15}$ are $(\Delta r)^+_{\min}\approx 1.0$, $(R\Delta\phi)^+_{\max}\approx 14.5$, and $(\Delta s)^+\approx 16.5$ (where the superscript "+" symbolizes normalization with viscous scales). From the previous analysis, as well as from similar analysis for the remaining combinations of flow rates and mesh densities under consideration, it can be inferred that the $M_{15}/M_{30}/M_{60}$ grids are of high quality and adequate resolution for DNS/LES/LES of the low/intermediate/high flow rates. Note that the Dynamic Smagorinsky model is used in our LES simulations.

The following time steps $dt_f$=10/10(10)/5(2.8)$\mu$s are used for the low/intermediate/high flow rates, leading to maximum CFL values that fluctuate around $0.75/1.02(1.10)/1.06(1.08)$. The numbers in parenthesis correspond to simulations with higher mesh densities (i.e. the intermediate and high flow rates are simulated via two meshes namely $M_{15}(M_{30})$ and $M_{30}(M_{60})$, respectively). Using the volume of the mouth-throat domain $V\approx 0.06L$ and the skeleton line length $L_{sk}\approx$26.4cm, we can extract a mean cross sectional area $A^m=V/L_{sk}$ with a value of $A^m\approx 2.27\text{cm}^2$. The associated mean bulk velocities $u_b^m=Q/A^m$ for the three flow rates are estimated to be $u_b^m\approx 1.1/2.2/4.4$m/s. These are 4.5 times lower than the respective

bulk velocities $u_b$ at the inlet. For each case, the effective simulation time (in which statistics are collected and particles are being tracked) is $T_{sim}$=2.4/2.4(2.4)/1.2(0.84)s such that a hypothetical fluid particle covers 10/20(20)/20(14) times the $L_{sk}$ length with the $u_b^m$ velocity.

The dispersed phase is simulated by the Lagrangian approach where particles are continuously released and tracked throughout the domain. One-way coupling is assumed between carrier fluid and dispersed aerosol phase. Spherical rigid particles with diameters $d_p$=0.5/1/2/4/6/8/10/15$\mu$m and density $\rho_p$=1000Kg/m$^3$ are released uniformly from the inlet. The particles experience drag, gravity ($g_z$=−9.81m/s$^2$), and buoyancy forces, while the interception mechanism is employed for the deposition. For each particle species a total number of 250000 particles are released uniformly across the first half of the simulation time, while they are being tracked for the full simulation time.

Details on the numerics of the code employed in the current study can be found in our most recent and related work (Stylianou *et al.*, 2016).

## RESULTS

Figure 6 unveils the dependency of particle Deposition Fraction (DF) on the flow rate, head position, and inhaler orientation. It is evident that the DF is minimally affected by the head position, with the head-up having slightly lower deposition values at all flow rates and inhaler orientations. The apparent lack of dependence of DF on the head position is a surprising result. To rule out the possibility that this could be linked to the rigid transformation of the mouth area between the three head positions, we plan to repeat the simulations using actual MRI-based geometries at the corresponding three head positions. For this purpose the MRI scans can be performed in upright body position, thus avoiding the difficulties associated with the supine body position. Regarding the flow rate, clearly the DF increases with increasing inhalation rate; a direct consequence of the increase of the inertia of particles (i.e. the Stokes number increases analogously with the flow rate). Concerning the inhaler orientation, at the low flow rate the 15$^o$-orientation reduces significantly the DF with respect to the other orientations. For the intermediate and high flow rates, the 30$^o$-orientation is slightly more effective than the 15$^o$-orientation for the smaller particles, but the opposite holds for the larger particles.

Since the head position does not have a profound impact on DF, we proceed with results related exclusively to the head-straight position. For all three inlet orientations, Figures 7, 8, and 9 highlight the average flow field patterns in the mouth region and depict the deposition sites for particles with diameters: $d_p$=8$\mu$m induced by the low flow rate, $d_p$=6$\mu$m induced by the intermediate flow rate, and $d_p$=4$\mu$m induced by the high flow rate, respectively. Note that the deposition sites of the high and intermediate flow rates are more dispersed with respect to the ones of the low flow rate, due to turbulent diffusion.

Clearly the orientation of the inlet determines the flow field structures in the mouth region, which in turn affect the particle deposition sites. Flow field patterns closer to the symmetry plane of the domain have a prominent jetal character, generating particle deposition sites at the apex of the *tongue* and/or at the center of the *soft palate* (i.e. posterior part of the roof of the mouth) via direct inertial impaction. On the contrary, flow field patterns further away from the symmetry plane of the domain have a strong vortical character, leading to particle deposition sites as the *sidewalls* via centrifugal inertial impaction. Evidently, by increasing the orientation angle of the inhaler, the deposition in the area of tongue and sidewalls is reduced while the deposition in the area of palate is increased. Clearly, there should be an optimum inhaler orientation angle asso-

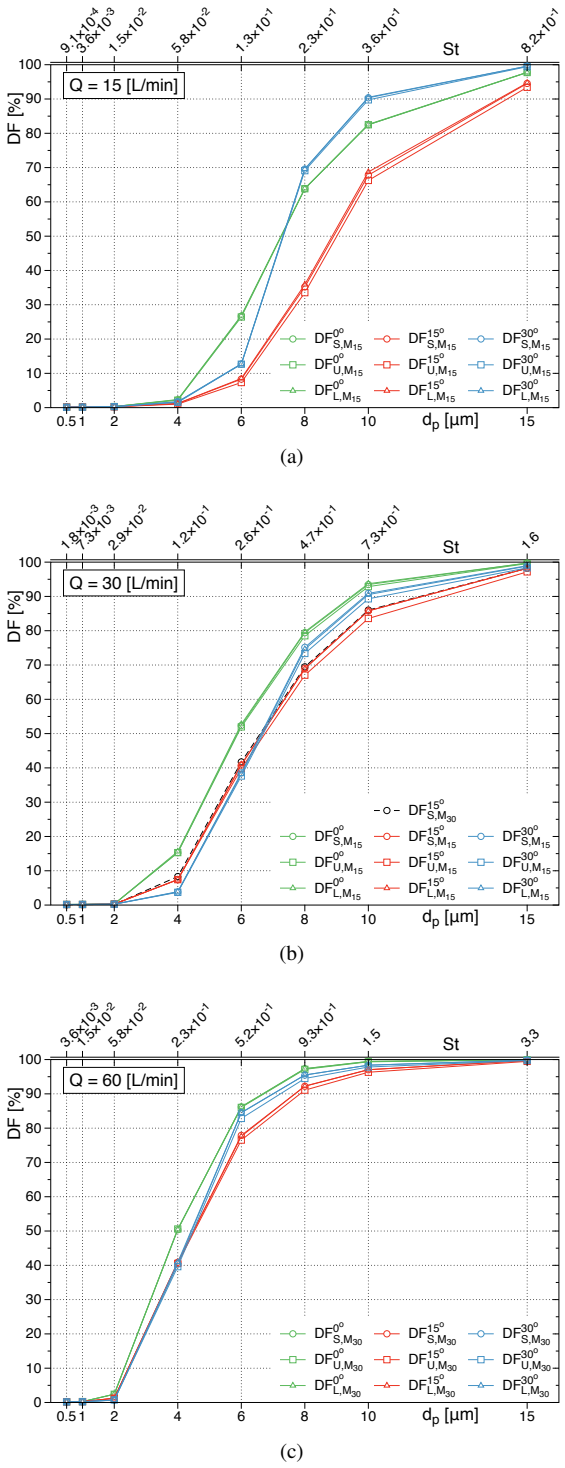


Figure 6: Deposition Fraction (DF) with respect to particle diameter $d_p$ (or Stokes number $St$=$\frac{\rho_p}{\rho_f}\frac{d_p^2}{R^2}\frac{Re_b}{36}$) for the three flow rates considered: (a) low, (b) intermediate, (c) high. For each flow rate, nine data sets are illustrated corresponding to the different combinations of head position (circles for head-straight, squares for head-up, triangles for head-left) and inhaler orientation (green for 0$^o$-orientation, red for 15$^o$-orientation, blue for 30$^o$-orientation). For the intermediate and high flow rates we are currently performing mesh independence study using the $M_{30}$ and $M_{60}$ meshes, respectively. In this study only the head-straight position is considered since the head position has small influence on the DF. At the moment, only one of these cases is completed and is shown with black dashed line.

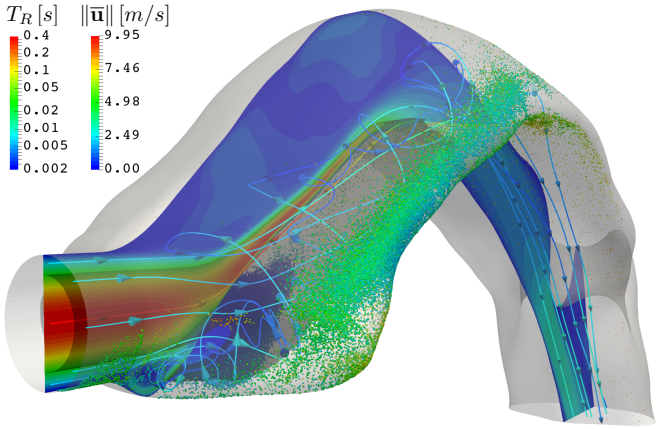


(a)

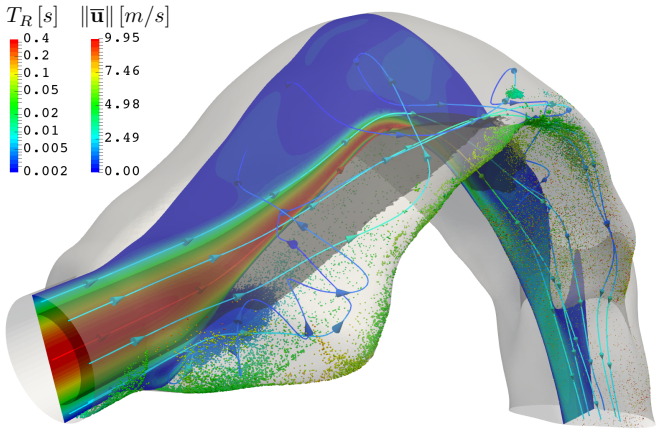


(b)

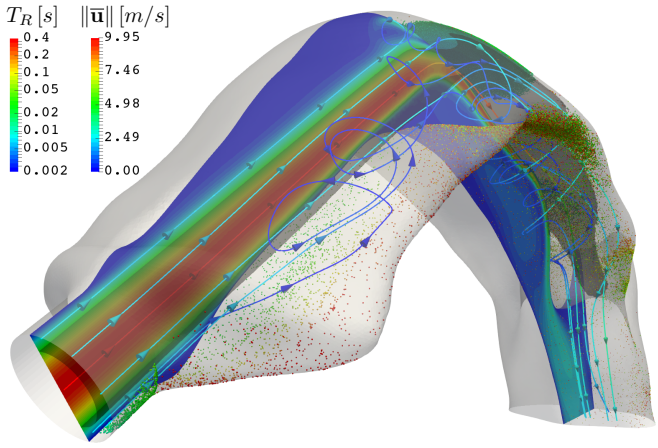


(c)

Figure 7: Deposition sites in the mouth region for particles with diameter $d_p$=8$\mu$m, induced by the low flow rate $Q$=15L/min, the head-straight position, and the three inhaler orientations: (a) 0$^o$-orientation, (b) 15$^o$-orientation, (c) 30$^o$-orientation. The particles are colored by their individual residence time $T_R$ (time interval between release and deposition). The contour plot at the symmetry plane of the geometry is based on the averaged velocity magnitude $\|\overline{\mathbf{u}}\|$. The streamlines are extracted from the averaged velocity vector field $\overline{\mathbf{u}}$, and colored by its magnitude $\|\overline{\mathbf{u}}\|$. An iso-surface of $\|\overline{\mathbf{u}}\|$=$u_b$ is illustrated with transparent light black color. The boundaries of the geometry are visible with transparent gray color.

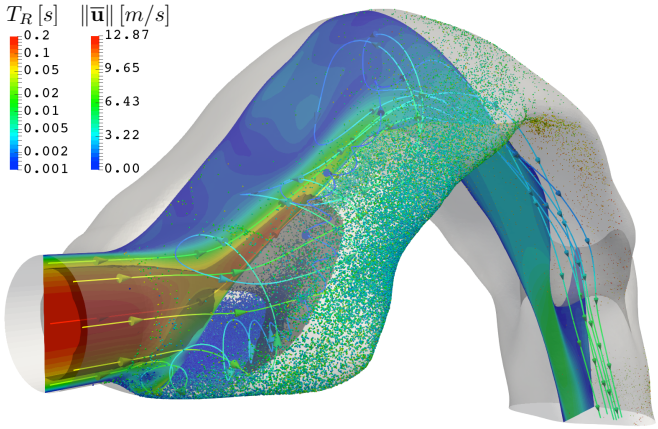


(a)

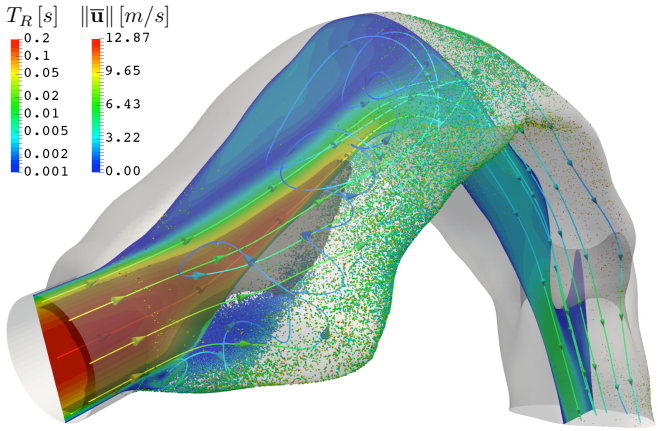


(b)

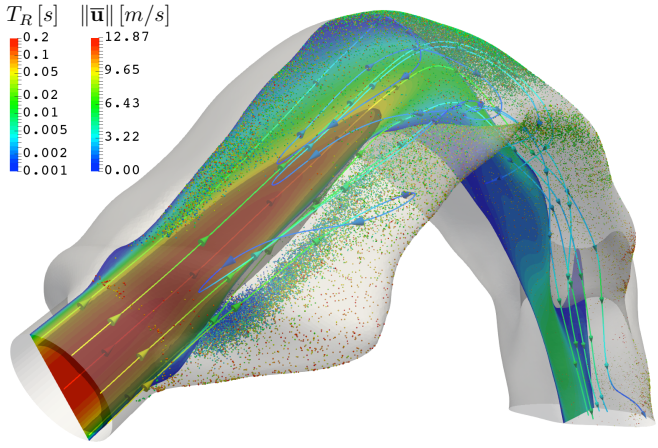


(c)

Figure 8: Same as in Figure 7, but for particles with diameter $d_p$=6$\mu$m, induced by the intermediate flow rate $Q$=30L/min.

ciated with minimal overall deposition in the mouth area.

## CONCLUSIONS

The current study highlights the effect of flow rate, head position, and inhaler orientation on the particle deposition of various micronized aerosols. Our results indicate that the deposition fraction is practically insensitive of the head position, while the flow rate and the inhaler orientation can significantly affect the deposition in the mouth-throat. For the specific geometry under consideration there is an optimum inhaler orientation angle that minimizes

the unwanted deposition in the mouth-throat. We envision inhalers with integrated features that force the users to hold the inhaler at the right orientation angle. This could contribute to a reduction of the side-effects and costs associated with DPI-delivered drugs.

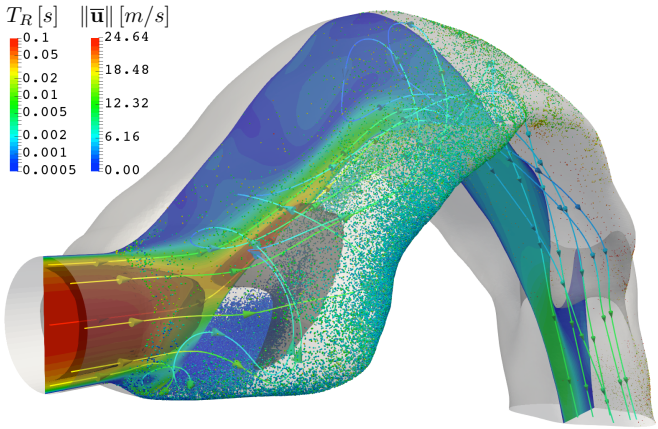


(a)

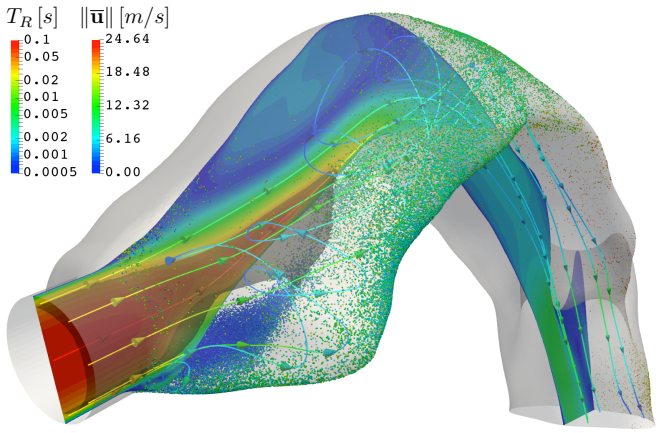


(b)

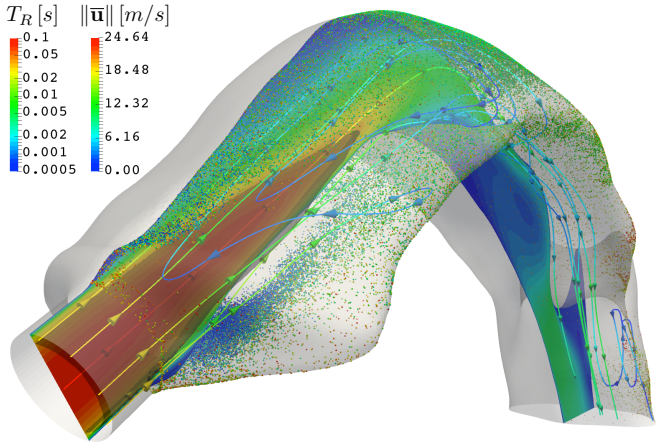


(c)

Figure 9: Same as in Figure 7, but for particles with diameter $d_p$=4$\mu$m, induced by the high flow rate $Q$=60L/min.

## FUTURE REFINEMENTS

We note that for the high flow rate a mesh independence analysis is pending, which will be available during the TSFP conference presentation. Furthermore, our results are under experimental evaluation by Emmace Consulting AB. In addition, we are currently investigating the effect of Saffman Lift force on the particles. Preliminary results indicate a small relative increase on the deposition. We plan to generalize our results by repeating the simulations using actual MRI-based geometries at the corresponding three head positions for more subjects. The shape of inlet mouthpiece, and the role of the teeth are also important factors that serve investigation.

## ACKNOWLEDGMENTS

The Prognosis Advanced Diagnostic Center is acknowledged for the MRI scans. In addition, the authors would like to acknowledge the financial support provided by COST-European Cooperation in Science and Technology, to the COST Action MP1404: Simulation and pharmaceutical technologies for advanced patient-tailored inhaled medicines (SimInhale).
Disclaimer: The content of this article is the authors responsibility and neither COST nor any person acting on its behalf is responsible for the use, which might be made of the information contained in it.

## REFERENCES

Behara, S.R.B., Longest, P., Farkas, D.R. & Hindle, M. 2014 Development and comparison of new high-efficiency dry powder inhalers for carrier-free formulations. *Journal of Pharmaceutical Sciences* **103** (2), 465–477.

de Boer, A.H., Gjaltema, D. & Hagedoorn, P. 1996 Inhalation characteristics and their effects on in vitro drug delivery from dry powder inhalers (Part 2). *International Journal of Pharmaceutics* **138** (1), 45–56.

DeHaan, W.H. & Finlay, W.H. 2004 Predicting extrathoracic deposition from dry powder inhalers. *Journal of Aerosol Science* **35** (3), 309–331.

Demoly, P., Hagedoorn, P., de Boer, A.H. & Frijlink, H.W. 2014 The clinical relevance of dry powder inhaler performance for drug delivery. *Respiratory Medicine* **108** (8), 1195–1203.

Patton, J.S., Fishburn, C.S. & Weers, J.G. 2004 The lungs as a portal of entry for systemic drug delivery. *Proceedings of the American Thoracic Society* **1** (4), 338–344.

Stylianou, F.S., Sznitman, J. & Kassinos, S.C. 2016 Direct numerical simulation of particle laden flow in a human airway bifurcation model. *International Journal of Heat and Fluid Flow* **61**, 677–710.

Usmani, O.S., Biddiscombe, M.F. & Barnes, P.J. 2005 Regional lung deposition and bronchodilator response as a function of $\beta$2-agonist particle size. *American Journal of Respiratory and Critical Care Medicine* **172** (12), 1497–1504.